

# Augmentation of Universal Potentials for Broad Applications

Joe Pitfield,\* Florian Brix, Zeyuan Tang, Andreas Møller Slavensky,  
Nikolaj Rønne, Mads-Peter Verner Christiansen, and Bjørk Hammer†  
*Center for Interstellar Catalysis, Department of Physics and Astronomy,  
Aarhus University, DK-8000 Aarhus C, Denmark*

Universal potentials open the door for DFT level calculations at a fraction of their cost. We find that for application to systems outside the scope of its training data, CHGNet[1] has the potential to succeed out of the box, but can also fail significantly in predicting the ground state configuration. We demonstrate that via fine-tuning or a  $\Delta$ -learning approach it is possible to augment the overall performance of universal potentials for specific cluster and surface systems. We utilize this to investigate and explain experimentally observed defects in the Ag(111)-O surface reconstruction and explain the mechanics behind its formation.

Keywords: Global Optimisation, Machine Learning, Neural Network Potentials, Gaussian Process Regression, Surface Reconstruction, Cluster

Atomic structure plays a crucial role in the understanding and development of new materials and technologies. A great many different compounds have structures which have been determined by experimental observation through a variety of techniques [2–6]. However, the configuration space of potential structures increases exponentially with degrees of freedom as we combine surfaces with adsorbates, defects, alloys and interfaces. Theoretical structure prediction offers the opportunity to screen and predict the structural properties of such systems. Studies of surface structure [7, 8], catalysis [9–12] and interface physics [13–16] provide valuable insight into not only the interesting material properties of these systems, but also the key limitations of first principles methods in addressing these ever more configurationally complex problems.

Machine learning models offer the ability to limit the amount of expensive first principles calculations performed, and the possibility of extending the results of small calculations to larger systems without the corresponding cubic[17] increase in cost common to density functional theory. Machine learning has been applied in a variety of ways to alleviate the computational workload of materials science: neural network potentials [18–24] and Gaussian process regression [25–31] for energetic evaluation, reinforcement[32–34] and active learning[16, 35] for candidate structure suggestion.

Such methods reduce the demand for expensive first principles calculations to be performed where the chosen model is well informed. If the model is not well informed, such as during the initialisation of such approaches, acquiring sufficient data often remains expensive. Recent interest has surrounded the utilisation of comprehensive structural databases such as the Materials Project[36], the OpenCatalyst Project[37] and PubChem[38] in training potentials which are broadly applicable. These so-called *universal potentials* theoretically remove the expensive initialisation step of any materials science workflow, promising orders of magnitude decrease in cost

for DFT accuracy calculations. Recent examples include M3GNet[39], MACE[40], AisNet[41], CHGNet[1] and DPA2 [42]. This work will focus on CHGNet, as it suggests strong performance with relatively few parameters ( $\sim 450,000$ ).

CHGNet is trained on the Materials Project dataset, which is dominated by structures which fall into the bulk regime. Unsurprisingly, CHGNet has been demonstrated to perform well when applied to materials in this realm[1]. However, the majority of device physics occurs in regimes where the materials deviate from perfect bulk crystals: interfaces have drastically varying conductivities [14, 43–48], defects play a key role in electronics [49–51], surfaces are defining in heterogeneous catalysis [52–54], and nanoparticulate phases are key in atmospheric[55] and astrochemical[56–58] contexts.

In this letter, we investigate with CHGNet the structural properties of two sets of materials involving either nano-particles or ultra-thin oxides on a surface. Varying system sizes and stoichiometries, we find for both types of materials that the universal potential is sufficiently accurate to identify the global minimum energy structures of some of the systems studied. However, we also find cases in which CHGNet lacks such accuracy. These cases form the basis for testing how to improve the pretrained CHGNet (v0.3.0). We pursue two avenues for this. Either we fine-tune the network, or we add an extra machine learning model to the potential prediction in what is known as  $\Delta$ -learning[59].

The letter is organized in the following manner: firstly we present two silicate clusters, and augment the CHGNet energy predictions where necessary, following either a fine-tuning or  $\Delta$ -learning strategy. Next, the effect of the augmentations is discussed as a function of the amount of data used. The letter proceeds to consider CHGNet predictions for ultra-thin oxides on the Ag(111) surface. Augmentation is found necessary for experimental consistency, and the  $\Delta$ -correction scheme is employed leading to the construction of a reliable model. Finally,

the model is applied to very large surface defect structures containing more than 1000 atoms.

Throughout this work, we will utilise optimization methods as implemented in the "Atomistic Global Optimization X" package, AGOX(v3.6.0)[60] that builds on the "Atomic Simulation Environment" (ASE)[61]. Density Functional Theory (DFT) calculations are performed in GPAW[62]. More details on the methods used are given in Section SII and Section SIV[63].

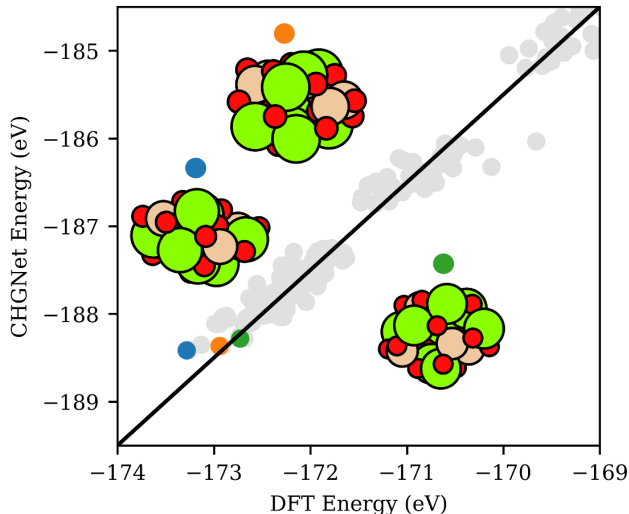


FIG. 1: Parity plot of CHGNet prediction vs DFT energy for four formula unit Olivine clusters. Three unique low-energy configurations are illustrated and corresponding datapoints indicated. The solid line is a guide to the eye. Green, tan and red spheres represent magnesium, silicon and oxygen atoms, respectively

Figure 1 presents three low energy configurations found for a silicate nano-particle with four olivine formula units, i.e.  $[\text{MgSi}_2\text{O}_4]_4$ . For these configurations, we find that CHGNet correctly predicts the same ordering as DFT[64]. This is evidenced by the parity plot of CHGNet versus DFT energies presented. We find similar DFT reproducibility behaviour of CHGNet for a range of other structures, see Section SI. This result demonstrates that despite CHGNet being trained largely on extended solid materials, it contains sufficient chemical insight so as to deal with the chemical consequences of compounds having finite size whereby many atoms end up in surface sites.

The offset of CHGNet energy to DFT energies apparent from Fig. 1 stems from the use of different DFT codes and DFT run-time parameters. The CHGNet architecture comes with 94 parameters, one for each atomic species, known as the *composition model*, which may be altered to accommodate such energy differences. Section SV discusses how to adjust the composition model pa-

rameters and eliminate the offset.

Using CHGNet for a wide variety of materials, we find occasional examples where it does not provide the same minimum energy configuration as found with DFT. An example of this is given in Fig. 2(a-c) that present three low-energy configurations of silicate nano-particles with four pyroxene formula units, i.e.  $[\text{MgSiO}_3]_4$  (PYR-4). In this case, the CHGNet model predicts the wrong stability ordering of the cluster configurations, as seen from the parity plot in Fig. 2(e). The structure preferred in CHGNet, Fig. 2(a), is hollow, while the one preferred in DFT[65], Fig. 2(c), is more compact.

To rationalize CHGNet's behavior for this system, we note that it relies on extrapolating the total energy of unknown systems by generalizing from local atomic descriptors in known systems. These descriptors result from graph-embedding in consecutive deep neural network layers, and predictions for certain motifs may be off, if these are not present in the training data.

We observe this effect whilst calculating the total dipole moments of these structures, which yields 1.22 and  $< 0.01$   $|e| \cdot \text{\AA}$ , for the CHGNet and DFT minima respectively. The much higher value of the CHGNet minimum occurs with the presence of magnesium coordinated magnesium in a triangular motif capped by a single oxygen, cf. upper part of structure in Fig. 2(a). We theorise that this motif has been incorrectly extrapolated from structures in which it correlates with stability.

Postulating thusly, the obvious solution is to augment the model with a collection of such data. In the following we shall take two approaches to such augmentation.

We first consider the option of fine-tuning CHGNet [66, 67]. Fine-tuning involves:

- Acquire  $N_{\text{sub}}$  pieces of data, that specify structures and corresponding DFT energies and forces.
- Split the data in training and validation data randomly in some desired ratio, e.g. 90:10.
- Complete a training step in which the network parameters are updated via backpropagation of the training data.
- Repeat steps until the model prediction accuracy on the validation set cannot be improved any further.

Figure 2(d) shows the energy prediction for the three low-energy cluster configurations of PYR-4 as a function of the amount of data,  $1 \leq N_{\text{sub}} \leq 2000$ , randomly extracted from an established dataset. Details of this dataset are given in the Section SVI.

As successively more data is used, the fine-tuned CHGNet indeed learns the relative ordering of the three low-energy cluster configurations, cf Fig. 2(d). Below 50 datapoints used, the fine-tuned CHGNet reacts turbulently to new data with predictions fluctuating in a jagged

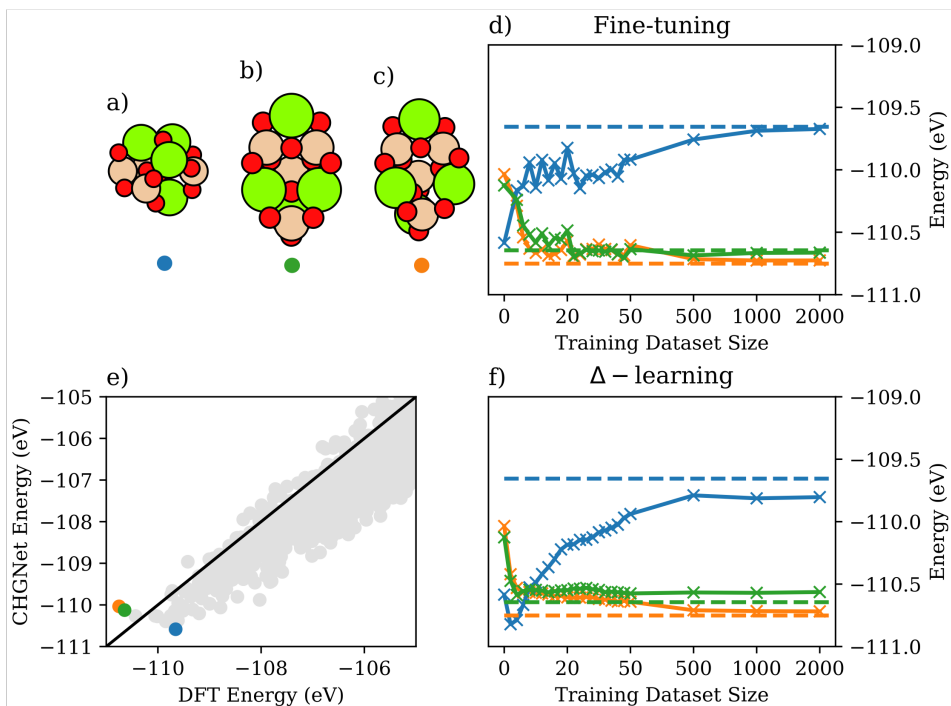


FIG. 2: (a-c) depict three low energy cluster configurations of PYR-4. (e) parity plot of the CHGNet vs DFT energies. (d) Fine-tuning prediction of energies with increasing data. (f)  $\Delta$ -model prediction of energies with increasing data. Structures (a-c) are color coded in all cases, with dashed lines indicating DFT energies.

manner. When these fluctuations settle for  $N_{\text{sub}} \geq 500$ , the fine-tuned CHGNet matches well the DFT energies of the respective structures.

Having seen that it is indeed possible to fine-tune CHGNet to learn system specific information and attain DFT-level accuracy, we now present an alternative approach:  $\Delta$ -learning. The motivation for developing a new approach stems from the fact that depending on the dataset size and the number of required epochs, the augmentation of a neural network via fine-tuning may be highly computationally costly, demanding expensive GPUs.

$\Delta$ -learning is an established machine learning approach in which one model learns "as much as it can" and a subsequent model learns the residual errors. Together, the two models are referred to as a  $\Delta$ -model.  $\Delta$ -learning has previously been successfully applied in the domain of molecular[68] and materials[69] modelling, amongst others [59, 70–76].

In the present context, we opt to use a Gaussian Process Regression (GPR) model for learning the residuals between the CHGNet and DFT values. We select GPR as an auxiliary model for its performance in the low data regime, both in terms of speed and reliability. Depending on hyper-parameters, a GPR may further excel in not correcting the CHGNet predictions outside the regions of the data used for the GPR training. This is unlike the situation in which a neural network is used as the aux-

iliary model, where corrective predictions could be more far reaching in impact.

In the  $\Delta$ -model approach we make predictions according to:

$$E_{\Delta\text{-model}}(\mathcal{S}) = E^{\text{CHGNet}}(\mathcal{S}) + \sum_i^N \Delta E^{\text{GPR}}(\mathbf{x}_i),$$

for an unknown structure,  $\mathcal{S}$ , with local atomic representations  $\mathbf{x}_i$ . The GPR model prediction for the residual can be seen in Section SIII.

We note, that it is instructive to think of a  $\Delta$ -model composed of a fixed NN and a trainable GPR model, as a GPR model with a prior given by the NN, which is concurrent with the language within our AGOX implementation.

The  $\Delta$ -model approach does not require the expensive GPU retraining of the neural network as was the case with the fine-tuning approach. In practice, we use a local SOAP-descriptor-based sparse GPR model, see Section SIII for more details[77, 78]. It would be equally viable to select any equivalently representative descriptor, including the intrinsic CHGNet features.

Figure 2(f) presents the prediction of the GPR-based  $\Delta$ -model as a function of the amount,  $N_{\text{sub}}$ , of data subsampled from the dataset. The silicate cluster stabilities predicted with the GPR-based  $\Delta$ -model are seen to smoothly tend towards the DFT values, i.e. they are not

jagged for  $N_{\text{sub}} \leq 50$ , and converge for  $N_{\text{sub}} \geq 500$ . The ordering becomes correct much earlier for the  $\Delta$ -model, being consistently so after as little as 10 data points. This evidences that the GPR-based auxiliary model is sufficiently versatile to learn the residuals in the space defined by the silicate clusters considered.

At this point, it is instructive to discuss the origin of the dataset. The dataset was constructed in consecutive cycles of structural searches followed by model augmentation. Further details are given in Section SVI. Here it suffices to highlight that such an active learning acquisition of training data is only computationally feasible if the model augmentation step is fast and stable with small additions of data. The differences in consistency between Figure 2(d,f) in the low data regime confirms that datasets can be more efficiently incorporated with the GPR-based  $\Delta$ -model. This leads to them being overall powerful options when augmenting the predictive power of CHGNet or similar universal potentials.

We now move to consider an application involving surface reconstructions, where we will demonstrate the use of the  $\Delta$ -model approach for system sizes not computationally accessible for DFT studies. Specifically, we shall consider three ultra-thin oxide phases that have been observed on Ag(111)[79, 80]. The phases are the  $c(4 \times 8)$ ,  $c(3 \times 5\sqrt{3})$ , and  $p(4 \times 5\sqrt{3})$ , that have 0.5, 0.4, and 0.375 oxygen/surface Ag coverages, respectively. For convenience, we shall refer to the three phases as phase I, II, and III, respectively.

Starting with phase I, inserts in Fig. 3(a) present its structure and two alternative structures found when searching in either the CHGNet or in the full DFT energy landscape. The parity plot displayed in Fig. 3(a) shows that CHGNet works quite well for this system. Moving to phase II in Fig. 3(b,c), the situation changes and now CHGNet predicts a structure with linear O-Ag-O motifs lining up in rows as the more stable, Fig. 3(b), while DFT has an elaborate structure with  $\text{Ag}_6$  triangles as the ground states, Fig. 3(c).

In order to remedy the identified deficiency and to resolve CHGNets prediction for the correct ground state structure for phase II, we collected, via 10 uncorrelated active learning campaigns, training data for 10 independent  $\Delta$ -models. Figure 3(d) shows the mean and uncertainty of predictions by these 10 models as a function of the amount of training data used. To put the approach to the test, we collected the data for the same cell as phase II itself, but for different stoichiometries, specifically omitting the stoichiometry containing the solution (see SI for details). Clearly, the models are capable of learning the correct ordering and energy difference of the two structures.

Finally, in Fig. 3(e-g) the situation for phase III is presented. Again, the pretrained CHGNet predicts a wrong ground state structure, Fig. 3(e), that does not have the  $\text{Ag}_6$  and  $\text{Ag}_{10}$  triangular motifs present in the

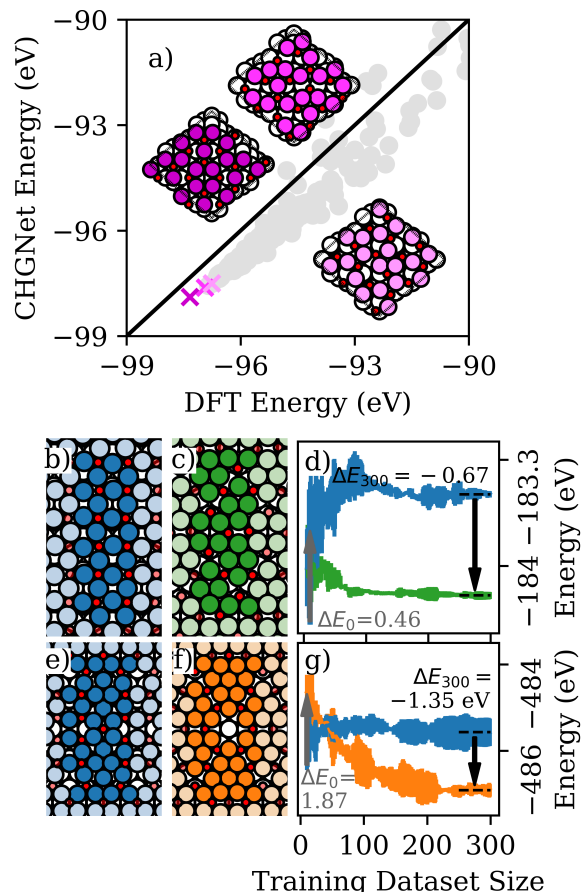


FIG. 3: (a) Parity plot of phase I structures, with colour coded insets depicting their correspondingly coloured points. DFT and CHGNet agree on the GM. (b) CHGNet GM for phase II. (c) DFT GM for phase II. (d)  $\Delta$ -model predictions for phase II. The DFT energy difference is calculated at -0.53 eV. (e) CHGNet GM for phase III. (f) DFT GM for phase III. (g)  $\Delta$ -model predictions for phase III. The DFT energy difference is -0.76 eV. In all depictions, red spheres represent oxygen, with all others indicating silver.

DFT ground state structure, Fig. 3(f). Now interestingly, the 10  $\Delta$ -models that were trained for phase II, when applied to phase III are able to predict the correct ordering and energy difference, as shown in Fig. 3(g). This demonstrates that the  $\Delta$ -models generalize well and opens for their application to more advanced materials problems where DFT calculations become prohibitively large.

In Fig. 4 we present such a case. The STM images in Fig. 4(a), obtained independently by the groups of Refs. 79 and 80, suggest the appearance of single rows of the phase III structure inside larger domains of phase II. These defect rows are observed to move dynamically at room temperature and their presence therefore cannot be ascribed to kinetic limitations. To assess the possibility of a thermodynamic origin of the rows we adopted a

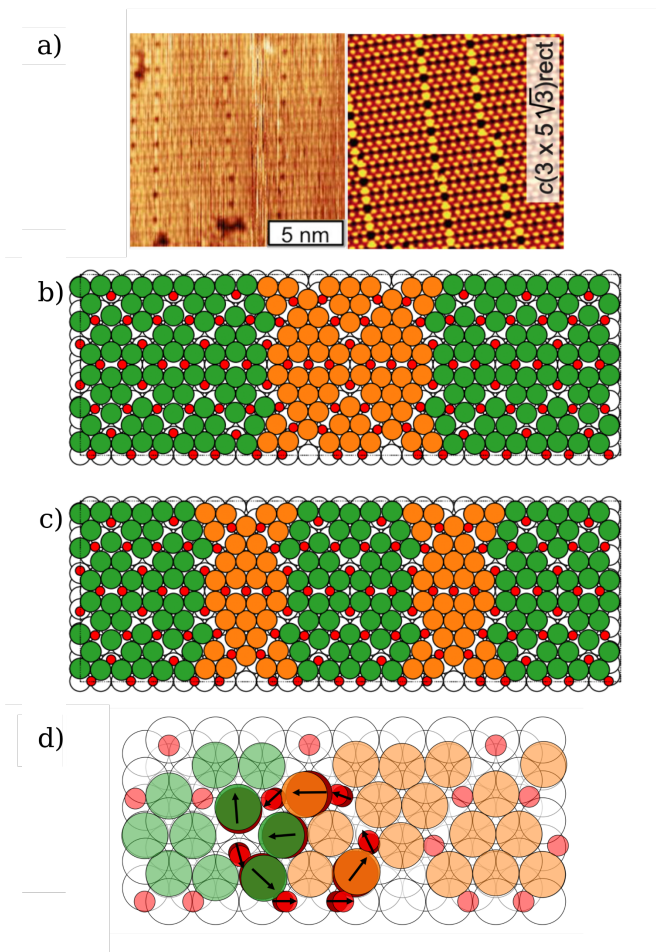


FIG. 4: a) Reproduction of STM images: Reprinted with permission from Ref. [80]. Copyright 2016 American Chemical Society, and from Ref. [79] under the Creative Commons Attribution 3.0 License, respectively. Both images depict the phase II ultra-thin oxide on Ag(111) under oxygen exposure, where single-width phase III stripes can be observed consistently. Schematics depicting b) neighbouring phase III cells, and c) dispersed III cells. d) Schematic of the relaxation undergone at the interface between phases II and III.

$\Delta$ -model selected from amongst those developed for Fig. 3. In Fig. 4(b,c) two systems are presented that explain why for instance the rows of phase III do not collapse to wider domains. In Fig. 4(b) two rows of phase III rows are adjacent to each other, and interfaced to phase II, while in Fig. 4(c) the two rows of phase III have dispersed in to being fully separated by phase II. With the augmented CHGNet model, we can calculate the energy change of this process, and find it to be preferred by 0.352 eV meaning that the interface energy between phase II and III is  $-0.176$  eV per  $5\sqrt{3}a/\sqrt{2}$  side length, where  $a$  is the lattice constant.

Figure 4(d) shows the considerable relaxations occurring at the interface between the two phases. Omitting the relaxations perpendicular to the interface plane the interface energy becomes essentially zero, leading us to conjecture that stress present within phase II is relieved at the interface and constitutes the driving mechanism for the presence of the rows of phase III defects within the large domains of phase II. The reason why the system does not evolve into alternating single rows of either phase, which would maximize the amount of favorable interfaces, is that this would also bring the overall oxygen coverage and hence chemisorption energy gain down, given the difference in O-coverage of phase II and III.

In conclusion, we have investigated the capability of a universal potential, CHGNet, in describing selected inorganic clusters and surfaces. In cases where the accuracy of the plain CHGNet model is insufficient to correctly order low-energy structures, we demonstrate that either fine-tuning or  $\Delta$ -learning offer a means to augment the model. We finally used a  $\Delta$ -learning augmented CHGNet model to identify and rationalize negative energy domain boundaries in the thin film oxides forming on Ag(111).

We acknowledge support by VILLUM FONDEN through Investigator grant, project no. 16562, and by the Danish National Research Foundation through the Center of Excellence “InterCat” (Grant agreement no: DNRF150).

\* [joepitfield@gmail.com](mailto:joepitfield@gmail.com)

† [hammer@phys.au.dk](mailto:hammer@phys.au.dk)

- [1] B. Deng, P. Zhong, K. Jun, J. Riebesell, K. Han, C. J. Bartel, and G. Ceder, *Nature Machine Intelligence* **5**, 1031 (2023).
- [2] P. F. Fewster, *Progress in crystal growth and characterization of materials* **48**, 245 (2004).
- [3] L. Stobinski, B. Lesiak, A. Malolepszy, M. Mazurkiewicz, B. Mierzwa, J. Zemek, P. Jiricek, and I. Bielloshapka, *Journal of Electron Spectroscopy and Related Phenomena* **195**, 145 (2014).
- [4] R. Černý, *Crystals* **7**, 142 (2017).
- [5] A. Gloystein, N. Nilius, J. Goniakowski, and C. Noguera, *The Journal of Physical Chemistry C* **124**, 26937 (2020).
- [6] S. S. Shields and J. A. Gupta, *Surface Science* **740**, 122403 (2024).
- [7] G. Gutiérrez, A. Taga, and B. Johansson, *Physical review B* **65**, 012101 (2001).
- [8] R. Zhang, L. Li, L. Frazer, K. B. Chang, K. R. Poepelmeier, M. K. Chan, and J. R. Guest, *Physical Chemistry Chemical Physics* **20**, 27456 (2018).
- [9] B. L. Hendriksen, M. D. Ackermann, R. Van Rijn, D. Stoltz, I. Popa, O. Balmes, A. Resta, D. Wermeille, R. Felici, S. Ferrer, *et al.*, *Nature chemistry* **2**, 730 (2010).
- [10] F. Polo-Garzon, Z. Bao, X. Zhang, W. Huang, and Z. Wu, *Acs Catalysis* **9**, 5692 (2019).
- [11] S. Chen, F. Xiong, and W. Huang, *Surface Science Reports* **74**, 100471 (2019).
- [12] E. A. D. Baker, J. Pitfield, C. J. Price, and S. P. Hepple-

- stone, *Journal of Physics: Condensed Matter* **34**, 375001 (2022).
- [13] C. Hill, R. Beach, and T. McGill, *Journal of Vacuum Science & Technology B: Microelectronics and Nanometer Structures Processing, Measurement, and Phenomena* **18**, 2044 (2000).
- [14] G. Schusteritsch, S. P. Hepplestone, and C. J. Pickard, *Physical Review B* **92**, 054105 (2015).
- [15] N. T. Taylor, F. H. Davies, I. E. M. Rudkin, C. J. Price, T. H. Chan, and S. P. Hepplestone, *Computer Physics Communications* **257**, 107515 (2020).
- [16] J. Pitfield, N. Taylor, and S. Hepplestone, *Physical Review Letters* **132**, 066201 (2024).
- [17] S. Mohr, L. E. Ratcliff, L. Genovese, D. Caliste, P. Boulanger, S. Goedecker, and T. Deutsch, *Physical Chemistry Chemical Physics* **17**, 31360 (2015).
- [18] J. Behler and M. Parrinello, *Physical review letters* **98**, 146401 (2007).
- [19] K. T. Schütt, H. E. Sauceda, P.-J. Kindermans, A. Tkatchenko, and K.-R. Müller, *The Journal of Chemical Physics* **148** (2018).
- [20] O. T. Unke and M. Meuwly, *Journal of chemical theory and computation* **15**, 3678 (2019).
- [21] J. Gastegger, F. Becker, and S. Günnemann, *Advances in Neural Information Processing Systems* **34**, 6790 (2021).
- [22] K. Schütt, O. Unke, and M. Gastegger, in *International Conference on Machine Learning* (PMLR, 2021) pp. 9377–9388.
- [23] I. Batatia, D. P. Kovacs, G. Simm, C. Ortner, and G. Csányi, *Advances in Neural Information Processing Systems* **35**, 11423 (2022).
- [24] S. Batzner, A. Musaelian, L. Sun, M. Geiger, J. P. Mailoa, M. Kornbluth, N. Molinari, T. E. Smidt, and B. Kozinsky, *Nature communications* **13**, 2453 (2022).
- [25] A. Denzel and J. Kästner, *The Journal of Chemical Physics* **148** (2018).
- [26] O.-P. Koistinen, V. Ásgeirsson, A. Vehtari, and H. Jónsson, *Journal of Chemical Theory and Computation* **16**, 499 (2019).
- [27] O.-P. Koistinen, V. Ásgeirsson, A. Vehtari, and H. Jónsson, *Journal of chemical theory and computation* **15**, 6738 (2019).
- [28] V. L. Deringer, A. P. Bartók, N. Bernstein, D. M. Wilkins, M. Ceriotti, and G. Csányi, *Chemical Reviews* **121**, 10073 (2021).
- [29] M. K. Bisbo and B. Hammer, *Physical Review B* **105**, 245404 (2022).
- [30] L. R. Merte, M. K. Bisbo, I. Sokolović, M. Setvín, B. Haggman, M. Shipilin, M. Schmid, U. Diebold, E. Lundgren, and B. Hammer, *Angewandte Chemie* **134**, e202204244 (2022).
- [31] Y. Hamamoto, T. N. Pham, M. K. Bisbo, B. Hammer, and Y. Morikawa, *Physical Review Materials* **7**, 124002 (2023).
- [32] M. S. Jørgensen, H. L. Mortensen, S. A. Meldgaard, E. L. Kolsbjerg, T. L. Jacobsen, K. H. Sørensen, and B. Hammer, *The Journal of Chemical Physics* **151** (2019).
- [33] Z. Zhou, S. Kearnes, L. Li, R. N. Zare, and P. Riley, *Scientific reports* **9**, 10752 (2019).
- [34] T. Gogineni, Z. Xu, E. Punzalan, R. Jiang, J. Kammeraad, A. Tewari, and P. Zimmerman, *Advances in Neural Information Processing Systems* **33**, 20142 (2020).
- [35] J. S. Smith, B. Nebgen, N. Lubbers, O. Isayev, and A. E. Roitberg, *The Journal of chemical physics* **148**, 241733 (2018).
- [36] K. A. Persson, B. Waldwick, P. Lazic, and G. Ceder, *Physical Review B* **85**, 235438 (2012).
- [37] L. Chanussot, A. Das, S. Goyal, T. Lavril, M. Shuaibi, M. Riviere, K. Tran, J. Heras-Domingo, C. Ho, W. Hu, *et al.*, *Acs Catalysis* **11**, 6059 (2021).
- [38] S. Kim, P. A. Thiessen, E. E. Bolton, J. Chen, G. Fu, A. Gindulyte, L. Han, J. He, S. He, B. A. Shoemaker, *et al.*, *Nucleic acids research* **44**, D1202 (2016).
- [39] C. Chen and S. P. Ong, *Nature Computational Science* **2**, 718 (2022).
- [40] I. Batatia, P. Benner, Y. Chiang, A. M. Elena, D. P. Kovács, J. Riebesell, X. R. Advincula, M. Asta, W. J. Baldwin, N. Bernstein, *et al.*, arXiv preprint arXiv:2401.00096 (2023).
- [41] Z. Hu, Y. Guo, Z. Liu, D. Shi, Y. Li, Y. Hu, M. Bu, K. Luo, J. He, C. Wang, *et al.*, *Journal of Chemical Information and Modeling* **63**, 1756 (2023).
- [42] D. Zhang, X. Liu, X. Zhang, C. Zhang, C. Cai, H. Bi, Y. Du, X. Qin, J. Huang, B. Li, *et al.*, arXiv preprint arXiv:2312.15492 (2023), <https://doi.org/10.48550/arXiv.2312.15492>.
- [43] T. J. Marks, *Angewandte Chemie International Edition in English* **29**, 857 (1990).
- [44] G. Chen, *Journal of Heat Transfer* **119**, 220 (1997).
- [45] C.-W. Nan, G. Liu, Y. Lin, and M. Li, *Applied Physics Letters* **85**, 3549 (2004).
- [46] N. Burger, A. Laachachi, M. Ferriol, M. Lutz, V. Toniazzo, and D. Ruch, *Progress in Polymer Science* **61**, 1 (2016).
- [47] S. Zhang, A. Hao, N. Nguyen, A. Oluwalowo, Z. Liu, Y. Dessureault, J. G. Park, and R. Liang, *Carbon* **144**, 628 (2019).
- [48] Q. Liu, F. Wang, W. Shen, X. Qiu, Z. He, Q. Zhang, and Z. Xie, *Ceramics International* **45**, 23815 (2019).
- [49] J. D. Bryan and D. R. Gamelin, *Progress in inorganic chemistry* **54**, 47 (2005).
- [50] B. I. Shklovskii and A. L. Efros, *Electronic properties of doped semiconductors*, Vol. 45 (Springer Science & Business Media, 2013).
- [51] C. Durand, X. Zhang, J. Fowlkes, S. Najmaei, J. Lou, and A.-P. Li, *Journal of Vacuum Science & Technology B* **33**, 02B110 (2015).
- [52] D. Rosenthal, *physica status solidi (a)* **208**, 1217 (2011).
- [53] W. Huang and W.-X. Li, *Physical Chemistry Chemical Physics* **21**, 523 (2019).
- [54] F. Zaera, *Coordination Chemistry Reviews* **448**, 214179 (2021).
- [55] P. Biswas and C.-Y. Wu, *Journal of the air & waste management association* **55**, 708 (2005).
- [56] Z. Tang, F. D. S. Simonsen, R. Jaganathan, J. Palotás, J. Oomens, L. Hornekær, and B. Hammer, *Astronomy & Astrophysics* **663**, A150 (2022).
- [57] A. P. Rasmussen, G. Wenzel, L. Hornekær, and L. H. Andersen, *Astronomy & Astrophysics* **674**, A103 (2023).
- [58] V. Poterya, I. S. Vinklársek, A. Pysanenko, E. Pluharova, and M. Fárník, *ACS Earth and Space Chemistry* **8**, 369 (2024).
- [59] R. Ramakrishnan, P. O. Dral, M. Rupp, and O. A. Von Lilienfeld, *Journal of chemical theory and computation* **11**, 2087 (2015).
- [60] M.-P. V. Christiansen, N. Rønne, and B. Hammer, *The Journal of Chemical Physics* **157** (2022).
- [61] A. H. Larsen, J. J. Mortensen, J. Blomqvist, I. E.

- Castelli, R. Christensen, M. Duřak, J. Friis, M. N. Groves, B. Hammer, C. Hargus, *et al.*, *Journal of Physics: Condensed Matter* **29**, 273002 (2017).
- [62] J. J. Mortensen, A. H. Larsen, M. Kuisma, A. V. Ivanov, A. Taghizadeh, A. Peterson, A. Haldrar, A. O. Dohn, C. Schäfer, E. Ö. Jónsson, *et al.*, *The Journal of Chemical Physics* **160** (2024).
- [63] See Supplemental Material at [*URL will be inserted by publisher*] for further details and discussions (see also Refs. [62, 65, 77, 78, 81–84]). The topics covered include: CHGNet out-of-the-box performance, DFT Settings, Local GPR, Global Optimisation, Composition Model, Silicate Dataset Creation, Silver Oxide Dataset Creation.
- [64] A. M. Slavensky, M.-P. V. Christiansen, and B. Hammer, *The Journal of Chemical Physics* **159** (2023).
- [65] A. M. Escatllar, T. Lazaukas, S. M. Woodley, and S. T. Bromley, *ACS Earth Space Chem.* **3**, 2390 (2019).
- [66] B. Deng, Y. Choi, P. Zhong, J. Riebesell, S. Anand, Z. Li, K. Jun, K. A. Persson, and G. Ceder, arXiv preprint arXiv:2405.07105 (2024).
- [67] B. Focassio, L. P. M. Freitas, and G. R. Schleder, *ACS Applied Materials & Interfaces* (2024), <https://doi.org/10.1021/acsami.4c03815>.
- [68] S. Käser, O. T. Unke, and M. Meuwly, *New Journal of Physics* **22**, 055002 (2020).
- [69] A. Nandi, C. Qu, P. L. Houston, R. Conte, and J. M. Bowman, *The Journal of Chemical Physics* **154**, 051102 (2021).
- [70] L. Hu, X. Wang, L. Wong, and G. Chen, *The Journal of Chemical Physics* **119**, 11501 (2003).
- [71] R. M. Balabin and E. I. Lomakina, *The journal of chemical physics* **131**, 074104 (2009).
- [72] M. Gillan, D. Alfè, A. Bartók, and G. Csányi, *The Journal of chemical physics* **139**, 244504 (2013).
- [73] P. Zaspel, B. Huang, H. Harbrecht, and O. A. von Lilienfeld, *Journal of chemical theory and computation* **15**, 1546 (2018).
- [74] S. Chmiela, H. E. Saucedo, K.-R. Müller, and A. Tkatchenko, *Nature communications* **9**, 3887 (2018).
- [75] H. E. Saucedo, S. Chmiela, I. Poltavsky, K.-R. Müller, and A. Tkatchenko, *The Journal of chemical physics* **150**, 114102 (2019).
- [76] M. Stöhr, L. Medrano Sandonas, and A. Tkatchenko, *The Journal of Physical Chemistry Letters* **11**, 6835 (2020).
- [77] A. P. Bartók, R. Kondor, and G. Csányi, *Physical Review B—Condensed Matter and Materials Physics* **87**, 184115 (2013).
- [78] N. Rønne, M.-P. V. Christiansen, A. M. Slavensky, Z. Tang, F. Brix, M. E. Pedersen, M. K. Bisbo, and B. Hammer, *The Journal of Chemical Physics* **157** (2022), 10.1063/5.0121748.
- [79] J. Schnadt, J. Knudsen, X. L. Hu, A. Michaelides, R. T. Vang, K. Reuter, Z. Li, E. Lægsgaard, M. Scheffler, and F. Besenbacher, *Phys. Rev. B* **80**, 075424 (2009).
- [80] J. Derouin, R. G. Farber, M. E. Turano, E. V. Iski, and D. R. Killelea, *ACS Catalysis* **6**, 4640 (2016).
- [81] J. P. Perdew, K. Burke, and M. Ernzerhof, *Physical review letters* **77**, 3865 (1996).
- [82] A. H. Larsen, J. J. Mortensen, J. Blomqvist, I. E. Castelli, R. Christensen, M. Duřak, J. Friis, M. N. Groves, B. Hammer, C. Hargus, E. D. Hermes, P. C. Jennings, P. B. Jensen, J. Kermode, J. R. Kitchin, E. L. Kolsbjerg, J. Kubal, K. Kaasbjerg, S. Lysgaard, J. B. Maronsson, T. Maxson, T. Olsen, L. Pastewka, A. Peterson, C. Rostgaard, J. Schiøtz, O. Schütt, M. Strange, K. S. Thygesen, T. Vegge, L. Vilhelmsen, M. Walter, Z. Zeng, and K. W. Jacobsen, *Journal of Physics: Condensed Matter* **29**, 273002 (2017).
- [83] L. Himanen, M. O. J. Jäger, E. V. Morooka, F. Federici Canova, Y. S. Ranawat, D. Z. Gao, P. Rinke, and A. S. Foster, *Computer Physics Communications* **247**, 106949 (2020).
- [84] J. Laakso, L. Himanen, H. Homm, E. V. Morooka, M. O. Jäger, M. Todorović, and P. Rinke, *The Journal of Chemical Physics* **158** (2023).

## Supplementary Information

Joe Pitfield,\* Florian Brix, Zeyuan Tang, Andreas Møller Slavensky,  
Nikolaj Rønne, Mads-Peter Verner Christiansen, and Bjørk Hammer†



## SI. OTHER EXAMPLES OF CHGNET SUCCESS OOTB

Success curves for global optimization of pyroxene with five and six formula units, using CHGNet as the target potential, are shown in figure S1. The best structures found in CHGNet indeed coincide with those found previously when using DFT as the target potential<sup>1</sup>. This testifies to the extrapolative power of the pretrained CHGNet.

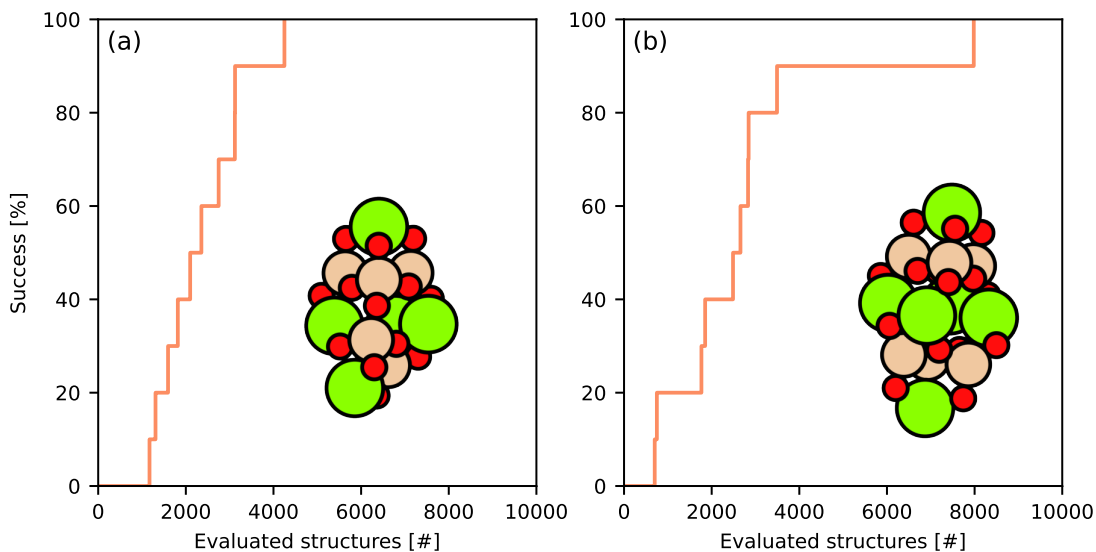


Figure S1: Success curves for finding the global energy minimum structures of pyroxene with (a) five and (b) six formula units. The target potential is CHGNet.

In Fig. 2, the results from a structural optimization for  $(2\sqrt{2} \times \sqrt{2})R45^\circ$  O-Cu(100) are considered. The search was done with DFT as the target potential, and subsequently the ideal and some defected structures were analysed with the pretrained CHGNet. The strong correlation demonstrates the predictive power of pretrained CHGNet for this system, where no augmentation is required.

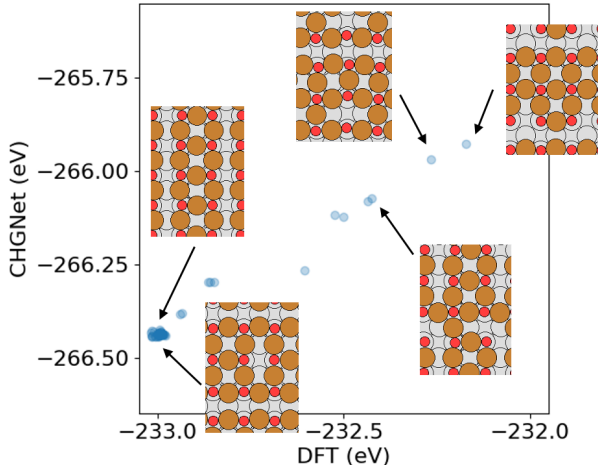


Figure S2: Parity plot of CHGNet versus DFT energies for various ideal and defected  $(2\sqrt{2} \times \sqrt{2})R45^\circ$  O-Cu(100) surface structures.

### SII. DFT SETTINGS

For all first-principles calculations performed throughout this work, we employed Density Functional Theory (DFT) as implemented in the GPAW package<sup>2</sup> and handled via the Atomic Simulation Environment package<sup>3</sup>. GPAW was used in the plane-wave mode with an energy cutoff of 500 eV. The XC-correlation functional adopted was the PBE<sup>4</sup>. The lattice constant of FCC-Ag was 4.15 Å. For modelling the Ag(111) surfaces, slabs of three (111) layers, with the two bottom layers fixed, were introduced. Forces were relaxed until being smaller than 0.025 eV/Å. For the Ag(111)- $c(4 \times 8)$ , Ag(111)- $c(3 \times 5\sqrt{3})$ , and Ag(111)- $p(4 \times 5\sqrt{3})$  surface unit cells, planar  $\mathbf{k}$ -point sets of  $(6 \times 6)$ ,  $(4 \times 4)$ , and  $(4 \times 2)$  were used.

### SIII. LOCAL GPR

In prior work, we introduced a sparse local GPR model<sup>5</sup>. We use a radial basis function kernel to evaluate covariance between local environments described through the SOAP representation<sup>6</sup>, as implemented in DDescribe<sup>7,8</sup>, given as

$$k(\mathbf{x}_i, \mathbf{x}_j) = A \exp\left(-\frac{|\mathbf{x}_i - \mathbf{x}_j|^2}{2l^2}\right). \quad (\text{S1})$$

$A$  and  $l$  are amplitude and length-scale hyperparameters. Predictions of local residual energies from the GPR is given by

$$\Delta E^{\text{GPR}}(\mathbf{x}_i) = \mathbf{k}_m(\mathbf{x}_i)C [\mathbf{E}^{\text{DFT}} - \mathbf{E}^{\text{CHGNet}}], \quad (\text{S2})$$

where  $\mathbf{x}_i$  is the local atomic representation of atom  $i$ ,  $\mathbf{k}_m(\mathbf{x}_i)$  is the kernel between  $\mathbf{x}_i$  and the inducing points  $X_m$ , the  $C$  matrix is the sparse version of the inverted covariance matrix and  $\mathbf{E}^{\text{DFT}} - \mathbf{E}^{\text{CHGNet}}$  is the training dataset residual energies. The  $C$  matrix is defined through the training dataset representations  $X_n$  and a set of inducing points  $X_m$  as

$$C = [K_{mm} + (LK_{nm})^T \Sigma_{nn}^{-1} (LK_{nm})]^{-1} (LK_{nm})^T \Sigma^{-1}, \quad (\text{S3})$$

where  $\Sigma_{nn}$  is a diagonal matrix of local noise,  $K_{mm} = k(X_m, X_m)$ ,  $K_{nm} = K_{mn}^T = k(X_n, X_m)$  and  $L$  the local energy correspondence matrix. The  $C [\mathbf{E}^{\text{DFT}} - \mathbf{E}^{\text{CHGNet}}]$  vector is pre-calculated during training.

An identical formulation can be constructed for implementing forces into the training data, where including gradients of the energy landscape invariably increases the accuracy of the model at the cost of decreasing the quantity of structures with which the GPR remains performative.

#### SIV. GLOBAL OPTIMIZATION

Searches were performed using parallel tempering as described in Ref. 9. 10 walkers were introduced with temperatures distributed exponentially from  $k_B T = 0.02$  eV to 2.0 eV. In every step, the structure of each walker was rattled randomly and relaxed in a local-descriptor sparse GPR model-based interatomic potential. The new structures were accepted according to the Metropolis Monte Carlo criterion. Rattle amplitudes were adjusted to achieve a 50% acceptance ratios. Swaps of structures between walkers were attempted for every 10 episodes. DFT calculations of the structures of the five lowest-temperature walkers were done for every 50 episodes, and the GPR model was updated. Runs were performed until the best structure, the putative GM structure, had been found multiple times for each stoichiometry.

The local descriptor used in the silicate cluster searches was SOAP-based with  $r_{cut} = 7$  Å,  $n_{max} = 3$ , and  $l_{max} = 2$ . The kernel was a radial basis function kernel (RBF) with length-scale  $= l = 20$  and prefactor  $= A = 1$ .

The local descriptor and kernel used in the silver oxide film searches were also SOAP-based and RBF-type, however with  $r_{cut} = 7$  Å,  $n_{max} = 3$ ,  $l_{max} = 2$ , length-scale  $l = 100$ , and prefactor  $A = 1$ .

## SV. COMPOSITIONAL MODEL

The CHGNet architecture includes a composition model that represents elemental one-body terms but crucially also average interaction energies for each element. This is a linear model

$$E_{comp}(S) = \sum_z n_z \epsilon_z,$$

where  $n_z$  is the number of atoms of species  $z$  in structure  $S$  and  $\epsilon_z$  is the learned average elemental energy for an atom of type  $z$ .

When training on DFT calculations produced with different settings than those of the original MPtrj training set, controlling this model is crucial. This translates into finding a new composition model,  $E_{comp}$ , which provides the best predictions when replacing the given composition model,  $E_{comp}^0$ , contained in the original CHGNet model,  $E_{CHG}^0$ . I.e. we seek the  $E_{comp}$  that best fulfills:

$$E_{DFT}(S) \approx E_{CHG}^0(S) - E_{comp}^0(S) + E_{comp}(S).$$

To refit this composition model on a new dataset we therefore do so with labels given by:

$$E_C^*(S) = E_{DFT}(S) - [E_{CHG}^0(S) - E_{comp}^0(S)],$$

where the term in the brackets is the CHGNet prediction of the difference from the average interaction energy. We fit the composition model by minimizing the least squares loss wrt.  $\epsilon_z$ :

$$L = \frac{1}{N} \sum_S ||E_C^*(S) - E_{comp}(S)||^2,$$

where  $N$  is the total number of structures in the training set. We use the labels  $E_C^*$  when refitting the composition model because if  $E_{DFT}$  was used, the new refitted model would essentially double count some parts of the interaction energy, as it would be accounted for both by the network and the composition model.

## SVI. SILICATE DATASET CREATION

The dataset for PYR-4 used in Fig. 2 was created in the follow way:

- Thirty independent search campaigns, following the global optimization methodology outlined in Section SIV, were conducted each producing about 100 structures.
- All structures were combined resulting in a total DFT dataset consisting of 3098 structures.
- DFT evaluations were performed after every 1000 episodes.

## SVII. SILVER OXIDE DATASET CREATION

The dataset for silver oxide thin films used in Fig. 3 was created in the follow way:

- Thin films of stoichiometry  $\text{Ag}_5\text{O}_{11}$ ,  $\text{Ag}_5\text{O}_{12}$ ,  $\text{Ag}_5\text{O}_{13}$ ,  $\text{Ag}_5\text{O}_{14}$ ,  $\text{Ag}_6\text{O}_{11}$ ,  $\text{Ag}_6\text{O}_{13}$ , or  $\text{Ag}_6\text{O}_{14}$  were considered while films of  $\text{Ag}_6\text{O}_{12}$  were neglected.
- For each stoichiometry ten independent search campaigns were conducted using the parallel tempering search strategy outlined in Section SIV. The GM structures found are depicted in Fig. S3
- The search results were combined into about 80 structures per stoichiometry, and a total 640 structures for all stoichiometries.

---

\* [joepitfield@gmail.com](mailto:joepitfield@gmail.com)

† [hammer@phys.au.dk](mailto:hammer@phys.au.dk)

<sup>1</sup> A. M. Escatllar, T. Lazaukas, S. M. Woodley, and S. T. Bromley, ACS Earth Space Chem. **3**, 2390 (2019).

<sup>2</sup> J. J. Mortensen, A. H. Larsen, M. Kuisma, A. V. Ivanov, A. Taghizadeh, A. Peterson, A. Haldar, A. O. Dohn, C. Schäfer, E. Ö. Jónsson, *et al.*, The Journal of Chemical Physics **160** (2024).

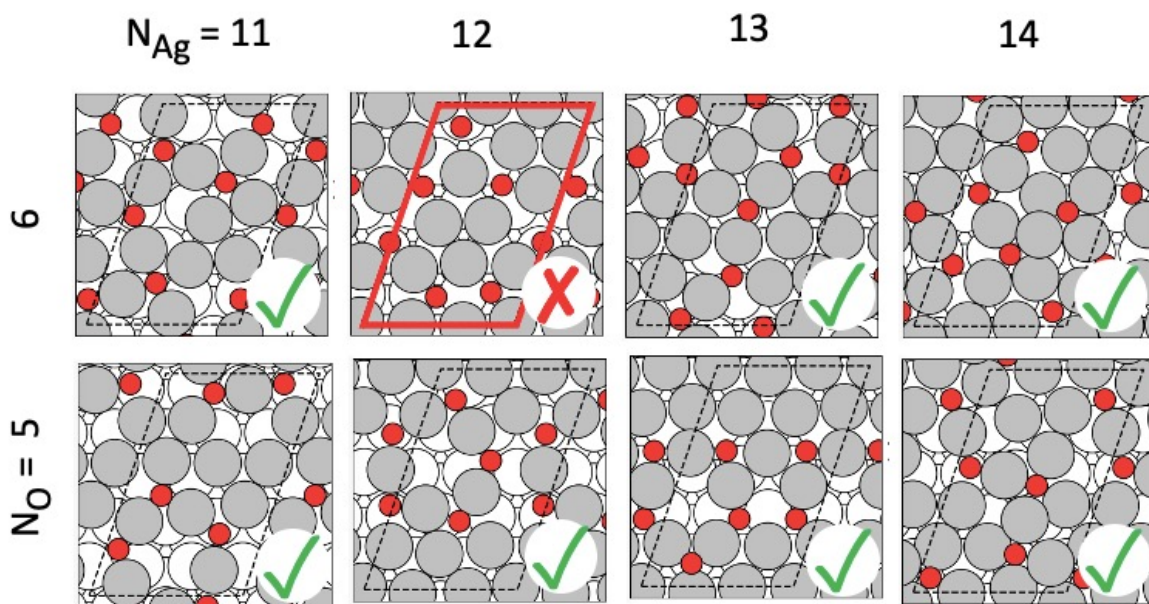


Figure S3: Images of the most energetically favourable structures found by a set of independent active learning runs over a range of stoichiometries for the O-Ag(111) surface reconstruction. The offset structure indicates that that calculation did not contribute to the final dataset employed in the main body of the letter, but did indeed correctly identify the dft ground state structure.

<sup>3</sup> A. H. Larsen, J. J. Mortensen, J. Blomqvist, I. E. Castelli, R. Christensen, M. Dułak, J. Friis, M. N. Groves, B. Hammer, C. Hargus, E. D. Hermes, P. C. Jennings, P. B. Jensen, J. Kermode, J. R. Kitchin, E. L. Kolsbjerg, J. Kubal, K. Kaasbjerg, S. Lysgaard, J. B. Maronsson, T. Maxson, T. Olsen, L. Pastewka, A. Peterson, C. Rostgaard, J. Schiøtz, O. Schütt, M. Strange, K. S. Thygesen, T. Vegge, L. Vilhelmsen, M. Walter, Z. Zeng, and K. W. Jacobsen, *Journal of Physics: Condensed Matter* **29**, 273002 (2017).

<sup>4</sup> J. P. Perdew, K. Burke, and M. Ernzerhof, *Physical review letters* **77**, 3865 (1996).

<sup>5</sup> N. Rønne, M.-P. V. Christiansen, A. M. Slavensky, Z. Tang, F. Brix, M. E. Pedersen, M. K. Bisbo, and B. Hammer, *The Journal of Chemical Physics* **157** (2022), 10.1063/5.0121748.

- <sup>6</sup> A. P. Bartók, R. Kondor, and G. Csányi, *Physical Review B—Condensed Matter and Materials Physics* **87**, 184115 (2013).
- <sup>7</sup> L. Himanen, M. O. J. Jäger, E. V. Morooka, F. Federici Canova, Y. S. Ranawat, D. Z. Gao, P. Rinke, and A. S. Foster, *Computer Physics Communications* **247**, 106949 (2020).
- <sup>8</sup> J. Laakso, L. Himanen, H. Homm, E. V. Morooka, M. O. Jäger, M. Todorović, and P. Rinke, *The Journal of Chemical Physics* **158** (2023).
- <sup>9</sup> M.-P. V. Christiansen, N. Rønne, and B. Hammer, *The Journal of Chemical Physics* **157** (2022).